PERGAMON

International Journal of Heat and Mass Transfer 44 (2001) 1039–1051

International Journal of HEAT and MASS TRANSFER

www.elsevier.com/locate/ijhmt

Thermal–hydraulic performance of small scale micro-channel and porous-media heat-exchangers

Pei-Xue Jiang *, Ming-Hong Fan, Guang-Shu Si, Ze-Pei Ren

Department of Thermal Engineering, Tsinghua University, Beijing 100084, People's Republic of China

Received 2 September 1999; received in revised form 21 February 2000

Abstract

Fluid flow and forced convection heat transfer in micro-heat-exchangers with either micro-channels or porous media have been investigated experimentally. The influence of the dimensions of the micro-channels on the heat transfer performance was first analyzed numerically. Based on these computations, deep micro-channels were used for the experimental studies reported here. The measured performance of both micro-channel and porous-media micro-heat-exchangers are compared with those of similar heat-exchangers tested by other researchers. It is shown that the heat transfer performance of the micro-heat-exchanger using porous media is better than that of the micro-heat-exchanger using micro-channels, but the pressure drop of the former is much larger. Over the range of test conditions, the maximum volumetric heat transfer coefficient of the micro-heat-exchanger using porous media was 86.3 MW/(m^3 K) for a water mass flow rate of 0.067 kg/s and a pressure drop of 4.66 bar. The maximum volumetric heat transfer coefficient of the micro-heat-exchanger using deep micro-channels was 38.4 MW/(m^3 K) with a corresponding mass flow rate of 0.34 kg/s and a pressure drop of 0.7 bar. Considering both the heat transfer and pressure drop characteristics of these heat-exchangers, the deep micro-channel design offers a better overall performance than either the porous media or shallow micro-channel alternatives.

Keywords: Micro-heat-exchangers; Micro-channels; Porous media; Volumetric heat transfer coefficient; Pressure drop

1. Introduction

In recent years, with the rapid progress in Micro-Electro-Mechanical Systems (MEMS), many micro-machining methods have been developed to build micro-devices such as micro-motors, micro-sensors, micro-mechanical gyroscopes, micro-pumps, micro-valves, micro-rockets, micro-gas-turbines, micro-heat-exchangers, etc. Micro-heat-exchangers and micro-channel heat sinks can be applied in many important fields: micro-electronics, aviation and aerospace, medical treatment, biological engineering, materials sciences, cooling of high temperature superconductors, thermal control of film deposition, cooling of powerful laser mirrors and other applications where lightweight, small heat-exchangers are required.

Compared with conventional heat-exchangers, the main advantage of the micro-heat-exchangers is their extremely high heat transfer area per unit volume. As a result, the overall heat transfer coefficient per unit volume can be as greater than 100 MW/(m^3 K), which is much higher than conventional heat-exchangers (1–2 orders of magnitude). Micro-channel heat-exchangers which are a common type of micro-heat-exchanger generally consist of many channels fabricated from very thin foils of silicon or metallic materials. Such foils can be used to form micro-channel heat sinks or can be welded together to form cross-flow, parallel-flow or counter-flow micro-heat-exchangers. The concept of "micro-channel heat sinks" was first introduced in 1981 by Tuckerman and Pease [1] who demonstrated experimentally that a heat flux of 1300 W/cm^2 can be continuously dissipated while maintaining a temperature

* Corresponding author. Tel.: +8610-62772661; fax: +8610-62770209.

E-mail address: jiangpx@te.tsinghua.edu.cn (P.-X. Jiang).

0017-9310/01/$ - see front matter
PII: S0017-9310(00)00169-1

Nomenclature

c	fluid specific heat, J/(kg K)
d	tube diameter, m
d_p	particle diameter, m
D_e	micro-channel equivalent diameter, $(= 2W_c h_c/(W_c + h_c))$, m
f	MCHE friction factor
f_e	MPHE friction factor
F	heat-exchanger total heat transfer surface area, m^2
G	mass flow rate, kg/s
$(Gc)_{min}$	minimum heat capacity rate, W/°C
h_c	channel depth, m
h_w	plate root section thickness (i.e., plate thickness minus channel depth), m
HE4	BR10 conventional plate heat-exchanger
K_c	pressure drop coefficient for sudden inlet contraction
K_e	pressure drop coefficient for sudden outlet expansion
K_F	heat-exchanger overall heat transfer coefficient, W/(m^2 K)
K_V	heat-exchanger volumetric heat transfer coefficient, W/(m^3 K)
L	channel length, m
MCHE	micro-channel heat-exchanger
MHE1	micro-channel heat-exchanger used in this research
MHE2	micro-porous heat-exchanger used in this research
MHE3	micro-channel heat-exchanger used by Kang [8] and Friedrich and Kang [10]
MPHE	micro-porous heat-exchanger
NTU	number of transfer units
Nu	Nusselt number
Pr	Prandtl number
Δp	pressure drop, Pa
q_w	wall heat flux, W/m^2
q''_z	average heat flux on the convection heat transfer surface at cross-section z, W/m^2
Q	heat transfer rate, W
Re	Reynolds number, $(= UD_e/v)$
Re_e	equivalent Reynolds number, $(= 2Ud_p/\ (3v(1-\phi)))$
Re_p	equivalent Reynolds number, $(= Ud_p/v)$
s_{xy}	coordinate for the wall perimeter at cross section z, mm
t	temperature, °C
$\Delta t_{m,N}$	log mean temperature difference for counter-flow heat-exchanger, °C
Δt_{max}	maximum temperature difference for both sides, °C
t_{fm}	fluid bulk temperature at cross-section z, °C
t_{wm}	average temperature on the convection heat transfer surface at cross-section z, °C
U	velocity, m/s
V	total volume, m^3
W_c	channel width, m
W_w	channel wall width, m
x, y, z	coordinates in numerical simulation, m

Greek symbols

α	heat transfer coefficient, W/(m^2 K)
ε	heat-exchanger effectiveness
φ	porosity $(= 0.47)$
ψ	heat-exchanger correction factor [31]
λ	thermal conductivity, W/(m K)
v	kinematic viscosity, m^2/s
ρ	fluid density, kg/m^3

Superscript

+	dimensionless quantity

Subscripts

c	channel
C	cold water
f	fluid
H	hot water
in	channel inlet
s	solid
w	wall
z	cross-section z

difference of less than 70°C. Since then, there have been many other related experimental works (e.g., [2–4]). The micro-heat-exchanger for exchanging heat between hot and cold fluids was first developed in 1985 by Swift et al. [5]. To facilitate fabrication and inlet and outlet flow conditions, most micro-channel heat-exchangers adopt a cross-flow arrangement. The dimensions and the heat transfer performance of different micro-heat-exchangers investigated previously are listed in Table 1.

Most micro-channel heat sinks use deep channels [2,3] (the micro-channel depth to width ratio is more than 1), while micro-channel heat-exchangers generally have shallow channels [5–10] (the depth to width ratio is less than 1). The reasons probably lie in the limits of fabrication, hardness and compactness of the heat transfer surfaces. Although decreasing the equivalent hydraulic diameter of the micro-channels can increase the heat transfer coefficient, the pressure drop is also greatly increased. Furthermore, the rate of increase of the pressure drop is far greater than that of the heat transfer coefficient. Both the heat transfer and the flow resistance should be considered in the design of micro-

Table 1
Dimensions and heat transfer performance of micro-heat-exchangers

References	W_c (mm)	h_c (mm)	h_c/W_c	K_F (kW/(m^2 K))	K_V (MW/(m^3 K))	Fluids
Cross et al. [6]	0.4	0.3	0.75	4.0	7	Water–water
Bier et al. [7]	0.1	0.078	0.78	22.8	324	Water–water
Kang et al. [8]	0.26 0.11	0.08	0.43	6.44	44.3	Water–water
Wild et al. [9]	0.103	0.07	0.68	1.0	11.2	Nitrogen–nitrogen

heat-exchangers. The equivalent hydraulic diameters of deeper channels for fixed channel width are relatively larger, so the flow resistance is relatively smaller while the heat transfer performance of deep channels is theoretically better than that of shallow channels according to Tuckerman [2], Keyes [11], Samalam [12], etc. Harms, et al. [13] experimentally showed that deeper channels provide better flow and heat transfer performance. However, there is little research related to the performance of two-fluid micro-channel heat-exchangers using deep channels, so more research work is needed.

Forced convection heat transfer in porous media has many important applications such as chemical particle beds, petroleum processing, transpiration cooling, solid matrix heat-exchangers, packed-bed regenerators, and heat transfer enhancement. Therefore, fluid flow and convection heat transfer in porous media have been received much attention for the past five decades, e.g., [14–21]. Previous results have shown that flow through porous media can greatly enhance the convection heat transfer [18,21]. There has been much research on tubular porous heat-exchangers [22,23], but the performance of plate porous heat-exchangers for exchanging heat between two fluids has received little attention. Jiang, et al. [24,25] theoretically analyzed the flow and heat transfer performance of small plate porous heat-exchangers. Since there is little relevant research work in the literature, this novel kind of micro-porous heat-exchanger needs further development and their flow and heat transfer performance need to be thoroughly investigated.

In this paper, the flow and heat transfer performances of a micro-channel heat-exchanger and a micro-porous heat-exchanger are theoretically and experimentally investigated and evaluated.

2. Experimental apparatus and data analysis

The experimental apparatus, shown schematically in Fig. 1, consisted of water tanks, pumps, a test section, regulator valves, accurate manometers, instrumentation to measure temperatures, an electric heater system and filters. The experimental system had both hot water and cold water loops. The hot water (distilled water) was circulated through a closed circuit. The cold water was supplied from a cold water tank. The test section contained either a micro-channel heat-exchanger (MCHE) or a micro-porous heat-exchanger (MPHE).

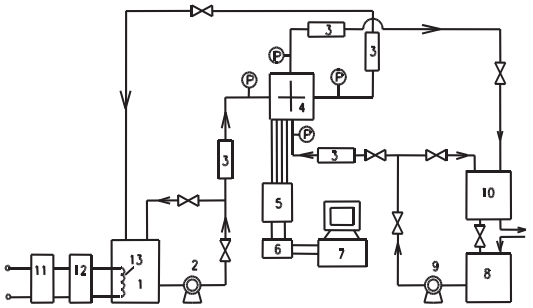

Fig. 1. Experimental apparatus: 1 – hot water tank; 2 – hot water pump; 3 – filter; 4 – test section; 5 – multiplexer; 6 – digital multimeter; 7 – personal computer; 8 – cold water tank; 9 – cold water pump; 10 – water tank; 11 – voltage stabilizer; 12 – voltage regulator; 13 – electric heater; P – manometer.

Micro-channels can be manufactured on sheet surfaces using either X-ray lithography technology (LIGA), silicon etching techniques, chemical etching, ion beam machining, diamond bit machining, precision mechanical sawing techniques or wire machining. Each method has advantages and disadvantages. In this research, the micro-channel heat-exchanger was fabricated from 0.7 mm thick pure copper plates on a wire cutting machine. The typical width and depth of the channels were 0.2 mm and 0.6 mm; the length and width of the sheets were both 21 mm; the active length of the channels was 15 mm with 38 channels per sheet; and the width of the fins between channels was 0.2 mm. The area density was 2895 m^2/m^3. Thirty sheets were machined and then cleaned using alcohol, acetone and an ultrasonic generator using water. A thin layer of soldering tin was coated on the back (without micro-channels) of each sheet. They were then stacked in a clamping fixture so that the channels in each sheet were oriented perpendicular to the channels in the two adjacent sheets. The stack was heated until the soldering tin melted (about 200°C). A scanning electron microscope photographic image of the micro-channel heat-exchanger is shown in Fig. 2(a). It is seen that the micro-channels fabricated by the wire cutting machine are not strictly rectangular and the surface is not smooth. Measurements using the scanning

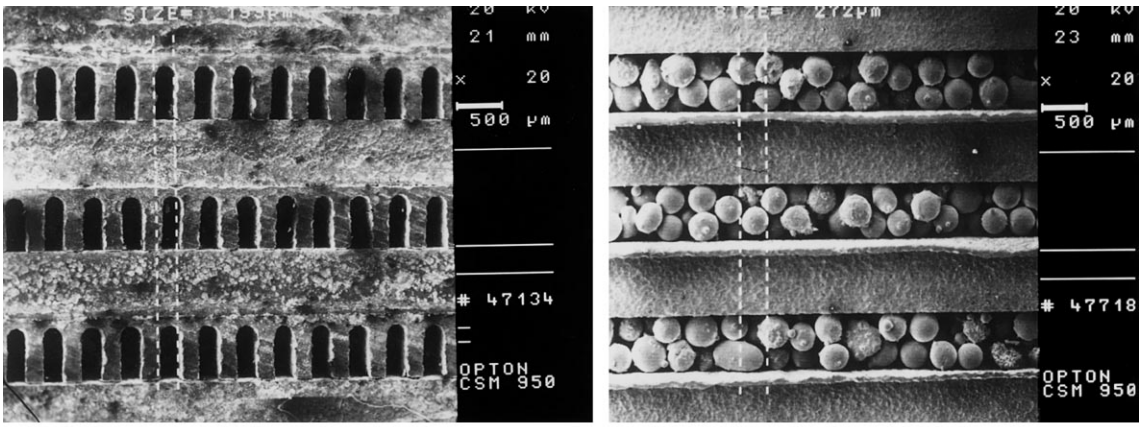

(a) (b)

Fig. 2. Scanning electron microscope photographic images of: (a) the MCHE; (b) the MPHE.

electron microscope showed that the surface roughness of the micro-channels was from 5.8 to 36.3 μm.

The micro-porous heat-exchanger was also fabricated from 0.7 mm thick pure copper plates by a wire cutting machine. The typical depth and the active length of the channels filled with porous media were 0.6 and 15 mm. The length and width of the sheets were both 21 mm; the average particle diameter was 0.272 mm; the porosity of the micro-porous heat-exchanger was 0.47; and the total area density including particles was 5011 m^2/m^3. The 30 sheets were sintered together with small copper particles to form a heat-exchanger. A scanning electron microscope photographic image of the micro-porous heat-exchanger is presented in Fig. 2(b).

The micro-heat-exchangers were packaged and sealed, Fig. 3, as described by Kang [8]. The heat-exchanger was slid into the fixture with the four corner slots filled with epoxy cement. Adjacent sides of the heat-exchanger were separated by the sealed corners. The fixture was bolted between two stainless steel plates and sealed by gaskets. Two mixers were placed at the outlets of hot and cold fluids in the fixture to increase the temperature measurement accuracy. The leakage inspection methods were described by Fan [26].

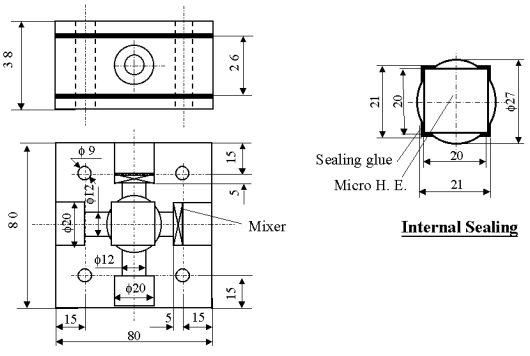

Fig. 3. Packaging and sealing of the micro-heat-exchangers.

Water was chosen as the working fluid. For each test, the hot and cold water flow rates, and the micro-heat-exchanger inlet and outlet fluid temperatures and pressures were measured at steady state. The temperatures were measured using four copper–constantan thermocouples, 0.2 mm diameter, connected through a multiplexer to a digital multimeter (HP34401A) and a personal computer. The thermocouples, calibrated using a constant-temperature oil bath, had an overall accuracy within ±0.2. The pressures at the inlet and outlet on both sides of the micro-heat-exchanger were measured using manometers with an accuracy of 0.25% of the full-scale range of 0.6 MPa. The flow rates were calculated by measuring the time period for a given fluid weight (e.g., 5 kg) to flow out of each side of the micro-heat-exchanger. For each experimental point, the flow rate was measured several times to determine an average value of the flow rate.

The relevant parameters were evaluated as:

Volumetric heat transfer coefficient

$$K_V = \frac{Q}{V\psi\,\Delta t_{m,N}}\ \mathrm{W/(m^3\ K)}. \tag{1}$$

Overall heat transfer coefficient

$$K_F = \frac{Q}{F\psi\,\Delta t_{m,N}}\ \mathrm{W/(m^2\ K)}. \tag{2}$$

Heat-exchanger effectiveness

$$\varepsilon = \frac{\Delta t_{\max}}{t_{H,in} - t_{C,in}}. \tag{3}$$

Number of transfer units

$$\mathrm{NTU} = \frac{FK_\mathrm{F}}{(Gc)_{\min}}. \tag{4}$$

Friction factor in MCHE [27]

$$f = \left(\frac{2\Delta p}{\rho U^2} - K_\mathrm{c} - K_\mathrm{e}\right)\frac{D_\mathrm{e}}{L}. \tag{5}$$

Friction factor in MPHE [27]

$$f_\mathrm{e} = \frac{\varphi^3}{6(1-\varphi)}\left(\frac{2\Delta p}{\rho U^2} - K_\mathrm{c} - K_\mathrm{e}\right)\frac{d_\mathrm{p}}{L}. \tag{6}$$

The experimental errors in the heat balance were less than 5%. The maximum error in the flow rate was less than 1.8%. The maximum error in the pressure measurement was 0.017 bar. The pressure drop in the experiments for the micro-channel heat-exchanger ranged from 0.033 to 0.9 bar, while for the porous media heat-exchanger the pressure drop in the experiments ranged from 0.23 to 4.66 bar depending on the mass flow rate. The dimensions of the micro-heat-exchanger structure including the width and depth of the channels, the width of the fins of the micro-channel heat-exchanger and the particle diameters of the micro-porous heat-exchanger were accurately determined using a scanning electron microscope. Analysis showed that the root-mean-square experimental uncertainties in the overall heat transfer coefficient, K_F, the volumetric heat transfer coefficient, K_V, the number of transfer units NTU, and the heat-exchanger effectiveness, ε, of the micro-heat-exchangers were 9.0%, 9.0%, 9.2% and 13.1%.

3. Results and discussion

3.1. Micro-channel heat-exchanger (MCHE)

3.1.1. Influence of the dimensions of the micro-channels on the thermal–hydraulic performance

A three-dimensional combined thermal conduction and forced convection heat transfer numerical analysis of the micro-channels was used to analyze the influence of the micro-channel size on the thermal–hydraulic performance of the micro-channel heat-exchanger and to provide theoretical basis for the design and optimization of its structure.

Mala and Li [28] found that the difference between the measured $\Delta p/\Delta l$ and correlation from conventional theory was small for micro-tube diameters more than 0.150 mm (with water as the working fluid). For micro-tube diameters from 0.050 to 0.203 mm, the higher flow resistance measured experimentally than that predicted by conventional theory may be explained by surface roughness effects and can be simulated numerically using a surface roughness–viscosity model. Harms, et al. [13] also concluded that for a multiple channel design (0.251 mm wide and 1.030 mm deep), the experimental friction factor agreed with the theoretical values reasonably well in both the laminar and turbulent regimes. The classical relations for local Nusselt number are appropriate and accurate for modeling micro-channel systems. Therefore, it is assumed that the continuity assumption is appropriate for the conditions studied in the present paper.

The physical model and coordinate system are depicted in Fig. 4. The governing equations, boundary conditions and numerical method were described by Fan [26]. It is assumed in the physical–mathematical model that the thermophysical properties of water are constant and the water is incompressible. The convection heat transfer conditions for adjacent micro-channels are assumed to be the same. The heat fluxes on the top and bottom surfaces of the micro-channels are assumed to be uniform and identical in the heat transfer region. The analysis assumes that the top and bottom micro-channel surfaces beyond the heat transfer region are insulated.

The convection heat transfer coefficient and Nusselt number were evaluated as:

Average convection heat transfer coefficient at cross-section z

$$\alpha_z = \frac{q''_z}{t_\mathrm{wm} - t_\mathrm{fm}}\ \mathrm{W/(m^2\,K)}. \tag{7}$$

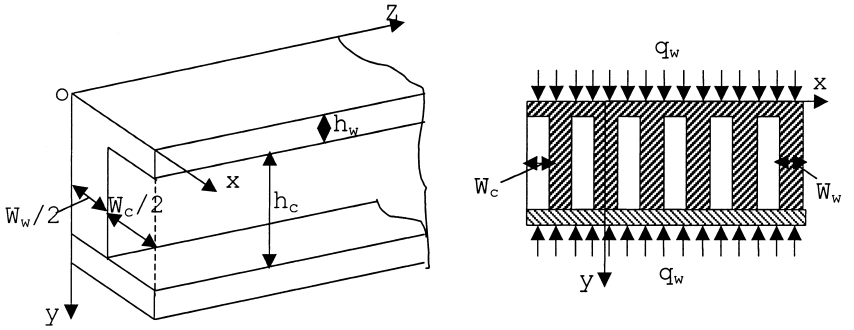

Fig. 4. Physical model and coordinate system for numerical simulation of micro-channel heat-exchanger.

Average Nusselt number at cross-section z

$$Nu_z = \frac{\alpha_z D_e}{\lambda_f}. \tag{8}$$

The numerical results were checked by comparison with known data and equations to verify the reliability of the physical–mathematical model and the numerical simulation program. The conditions for the numerical calculations were $W_c = 0.2$ mm, $h_c = 0.6$ mm, $W_w = 0.2$ mm, $h_w = 0.1$ mm, $L = 20$ mm, $t_{in} = 15$°C, $q_w = 270$ kW/m^2, $\lambda_s = 398.1$ W/(m K), $\lambda_f = 0.6$ W/(m K), $Pr = 7.0$. The cross-sectional average Nusselt number in the flow direction is presented in Fig. 5. The solid line is from the correlation for the thermal entry region of circular tubes for constant heat flux boundary conditions recommended by Petukhov, et al. [29]

$$Nu_z = 4.36 + 1.31\left(RePr\frac{d}{z}\right)^{1/3} \exp\left(-13\sqrt{\frac{z}{RePrd}}\right), \quad \frac{z}{RePrd} > 0.001. \tag{9}$$

The numerical results of Wibulswas [30] for the thermal entry region of a rectangular tube with $h_c/W_c = 3$ for constant heat flux boundary conditions are also given in Fig. 5. The present numerical results are very close to the numerical results of Wibulswas [30] and the results calculated using Eq. (9), which indicates that the numerical simulation agrees well with classical theory.

Fig. 6 shows the distribution of the local heat flux along the perimeter on the convection heat transfer surface at the cross-section $z = 15.0$ mm from the channel inlet. Here $s_{xy} = -0.2 \sim 0.1$ mm represents half of the height of the micro-channel ($s_{xy} = -y + 0.2$), while $s_{xy} = 0.1 \sim 0.2$ mm represents half the width of the micro-channel ($s_{xy} = x$), $s_{xy} = 0.1$ mm represents the corner. Obviously, the convection heat transfer at the middle of the vertical edge of the micro-channel is the greatest, whereas the convection heat transfer at the corner of the micro-channel is the least due to stagnation. The heat transfer along the bottom of the micro-channel is much less than the convection heat transfer along the fins (the vertical surface of the micro-channel). For this reason, the present work uses deep micro-channels.

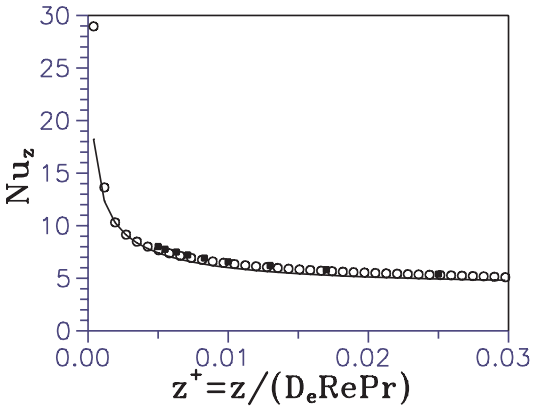

Fig. 5. Cross-sectional average Nusselt number along the flow direction: ◯ – numerical results of the present paper; ■ – numerical results in [30]; —— Eq. (9).

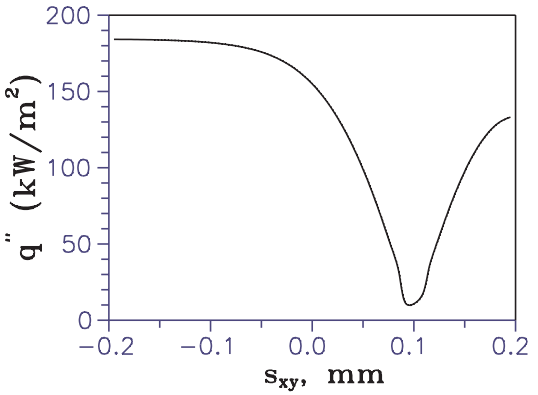

Fig. 6. Distribution of the local heat flux on the wall of the cross-section $z = 15.0$ mm.

The purpose of the numerical calculation, as above mentioned, was to study the effect of the micro-channel dimensions on the thermal–hydraulic performance. Although the mathematical–physical model does not perfectly model the actual processes in the micro-channel heat-exchanger, the numerical investigation of the influence of dimensions on the fluid flow and convection heat transfer can help optimize micro-heat-exchangers.

Due to the limitations of the wire machining technology, the minimum channel width is 0.2 mm, whereas the channel can be any depth. Therefore, six different channel depths (0.1, 0.2, 0.4, 0.6, 0.8, and 1.6 mm) were used for the numerical calculations with the assumption of $W_c = W_w = 0.2$ mm and $h_w = 0.1$ mm. For these conditions, the pressure drop variation in the micro-channels with channel depth is presented in Fig. 7(a) for $Re = 224$. The pressure drop variation with depth is significant, with deeper channels having less pressure drop. The relationship between the channel depth and the average convection heat transfer coefficient, Fig. 7(b), is not monotonic, for $h_c < 0.4$ mm the average convection heat transfer coefficient decreases with increasing channel depth; whereas for $h_c > 0.4$ mm the average convection heat transfer coefficient increases with increasing channel depth. The ratio of the volumetric heat transfer coefficient and the pressure drop, $K_V/\Delta p$ increases with increasing channel depth, Fig. 7(c); therefore, deep channels have an advantage. The results in Fig. 7 show that when $h_c > 0.6$ mm, the

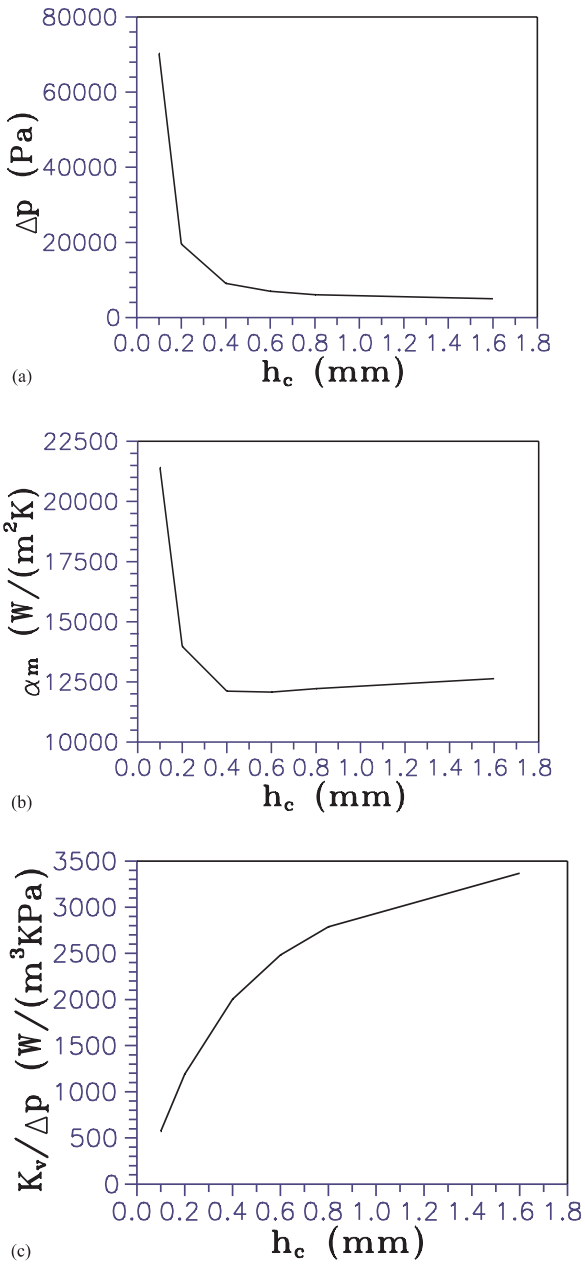

Fig. 7. Variation of pressure drop (a) and average convection heat transfer coefficient (b) in a micro-channel with channel depth and effect of channel depth on the ratio of the volumetric heat transfer coefficient and the pressure drop (c).

pressure drop decrease, the average convection heat transfer coefficient increase and the increase of the ratio $K_V/\Delta p$ are not significant. Therefore, since very deep channels will be difficult to manufacture and will increase the micro-heat-exchanger size, the channel depth was selected as $h_c = 0.6$ mm. However, optimization of the micro-heat-exchanger dimensions should be studied further.

3.1.2. Experimental results and analysis

The pressure drop in the micro-channel heat-exchanger is plotted as a function of velocity in the micro-channel in Fig. 8. Here, MHE1 and MHE2 represent the micro-channel heat-exchanger and the micro-porous heat-exchanger used in this research, MHE3 represents the micro-channel heat-exchanger used by Kang [8] and Friedrich and Kang [10], and HE4

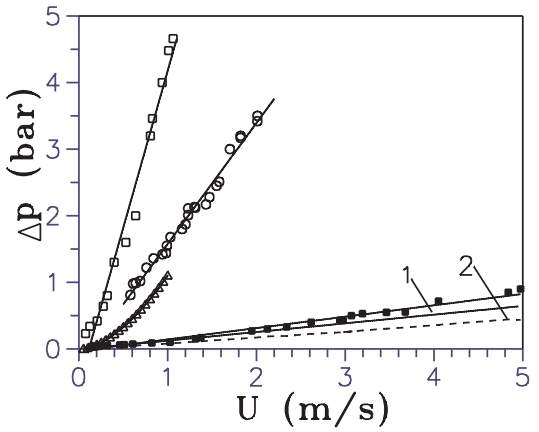

Fig. 8. Variation of pressure drop with velocity: ■ – MHE1; □ – MHE2; ◯ – MHE3; △ – HE4: 1 – numerical results; 2 – Eq. (10).

represents the conventional plate heat-exchanger (BR10). The geometric parameters for HE4 are given by Fan [26]. The water flow rate in the micro-channel heat-exchanger ranged from 0.0093 to 0.34 kg/s, the corresponding velocities were 0.13–4.97 m/s and the pressure drop increased from 0.033 to 0.9 bar. Fig. 8 also presents the numerical results and the value from Eq. (10) for fully developed laminar flow. Fig. 9 compares the friction factor, f, calculated from the experimental data for the micro-channel heat-exchanger and predicted by the friction factor equations for fully developed laminar (Eq. (10)) and turbulent (Eq. (11)) flow in smooth rectangular channels:

$$f = 68.35/Re, \tag{10}$$

$$f = 0.31/Re^{0.25}. \tag{11}$$

As shown in Figs. 8 and 9, the experimental values of Δp and f are larger than the values predicted numerically and by Eqs. (10) and (11) because the channels used in the research have large relative roughness (about 1.9–12.1%) and the roughness is non-uniform. Moreover, since the micro-channels are hydrodynamically short in most cases, the flow is in the hydrodynamic entrance region and the relative experimental uncertainty in the friction factor f was great for the small flow rates. As noted by other researchers, e.g., Wu and Little [4], Harms, et al. [13] and Mala and Li [28], the transition from laminar to turbulence in micro-channels occurs much earlier (in the present research $Re_{cr} \approx 600$). The early transition from laminar to turbulence may occur because of the sudden inlet contraction and the large relative roughness and the asymmetric roughness. The friction factor f can be correlated with Re as follows

$$f = 1639/Re^{1.48} \quad (Re < 600), \tag{12}$$

$$f = 5.45/Re^{0.55} \quad (600 < Re < 2800). \tag{13}$$

The discrepancy between Eqs. (12) and (13) and the experimental data is less than ±10%.

The overall volumetric heat transfer coefficient for the micro-channel heat-exchanger, Fig. 10, increases with increasing hot water mass flow rate when the cold water mass flow rate was fixed. For very small hot water mass flow rates, the volumetric heat transfer coefficients are independent of the cold water flow rate since the convective thermal resistance on the hot side is dominant and restricts the overall thermal performance of the heat-exchanger.

Fig. 11 shows the volumetric heat transfer coefficients in the micro-heat-exchanger as a function of velocity for equal hot and cold side mass flow rates. The maximum water flow rate in the micro-channel heat-exchanger was

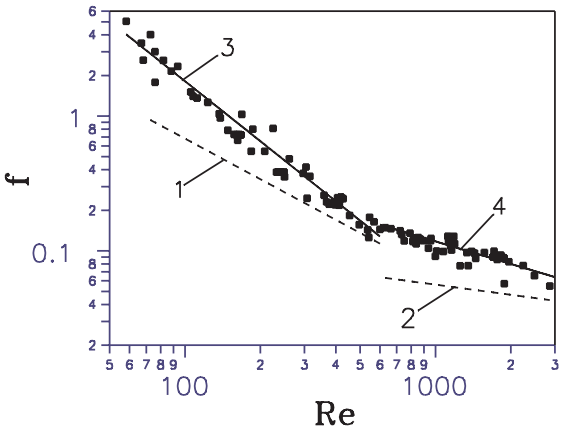

Fig. 9. MCHE friction factor: 1 – Eq. (10); 2 – Eq. (11); 3 – Eq. (12); 4 – Eq. (13); ■ – experimental data.

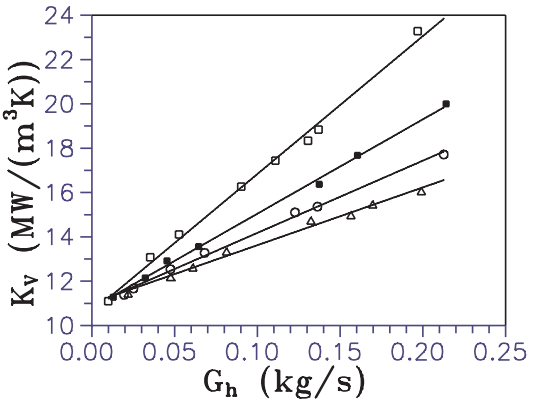

Fig. 10. Volumetric heat transfer coefficient for the MCHE for various cold water flow rates G_C [kg/s]: △ – 0.034; ◯ – 0.056; ■ – 0.105; □ – 0.213.

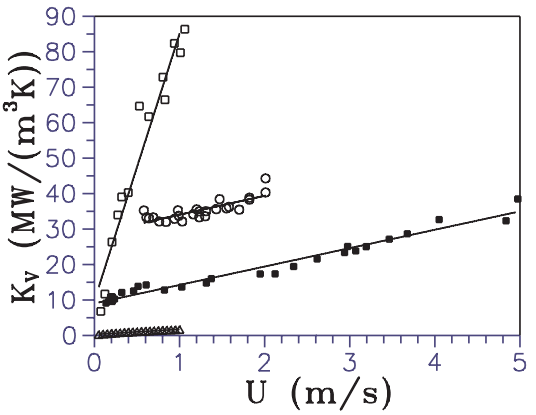

Fig. 11. Volumetric heat transfer coefficients: ■ – MHE1; □ – MHE2; ○ – MHE3; △ – HE4.

0.34 kg/s, the corresponding average velocity was 4.97 m/s. The maximum volumetric heat transfer coefficient was 38.5 MW/(m^3 K) and the maximum overall heat transfer coefficient was 13.3 kW/(m^2 K). The heat transfer will be compared to the other heat-exchangers in the following section.

Fig. 12 relates the average Nusselt number and the dimensionless length X^+. The average Nusselt number decreases from 12.9 to 3.0 with increasing X^+. Two different flow regimes are seen in the Nu–X^+ relationship: for $X^+ < 0.05$ the average Nusselt number decreases sharply with increasing X^+; whereas for $X^+ > 0.05$ the average Nusselt number decreases very slowly with increasing X^+. The different heat transfer regimes are due to the flow regimes and the thermal entry effect. The relationships between Nu and X^+ can be correlated as:

$$Nu = 0.52(RePrD_e/L)^{0.62}, \quad (X^+ < 0.05), \tag{14}$$

$$Nu = 2.02(RePrD_e/L)^{0.31}, \quad (X^+ > 0.05). \tag{15}$$

The discrepancy between Eqs. (14) and (15) and the experimental data is less than ±10%.

Fig. 13 presents the heat-exchanger effectiveness of the micro-channel heat-exchanger as a function of number of transfer units, NTU, for equal hot and cold side mass flow rates. For a single-pass, cross-flow heat-exchanger with both fluids unmixed, the heat-exchanger effectiveness is [31]

$$\varepsilon = 1 - \exp\{\mathrm{NTU}^{0.22}[\exp(-\mathrm{NTU}^{0.78}) - 1.0]\}. \tag{16}$$

The experimental data for ε is a little higher than predicted by Eq. (16) possibly because the hot and cold water mass flow rates in the experiments are not exactly the same. The differences between the experimental data for the heat-exchanger effectiveness and the calculated results using Eq. (16) are less than 5%.

3.2. MPHE

The pressure drop in the MPHE is shown in Fig. 8 as a function of velocity (MHE2). The water flow rate in the MPHE ranged from 0.005 to 0.067 kg/s with corresponding average velocities of 0.074–1.06 m/s and pressure drops of 0.23–4.66 bar. For the same flow rate, the pressure drop in the MPHE is much larger than in the MCHE.

Fig. 14 compares the friction factor, f_e, calculated from the experimental data and that predicted by the friction factor equation for flow in porous media channels [32]

$$f_e = 36.4/Re_e + 0.45 \quad (Re_e < 2000). \tag{17}$$

The friction factor initially decreases very quickly with increasing Re_e and then more slowly. The MPHE has only 2–3 layers of particles in a cross-section, whereas

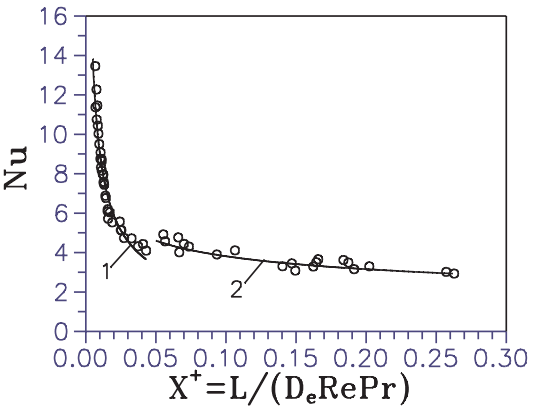

Fig. 12. Average Nusselt number for MCHE: ○ – experimental results; 1 – Eq. (14); 2 – Eq. (15).

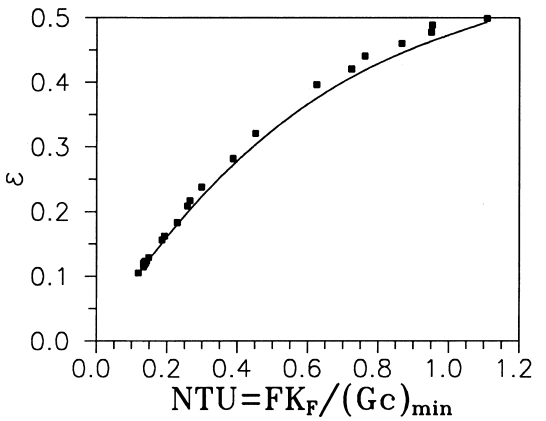

Fig. 13. Effectiveness of the cross-flow MCHE: ■ – experimental results; —— Eq. (16).

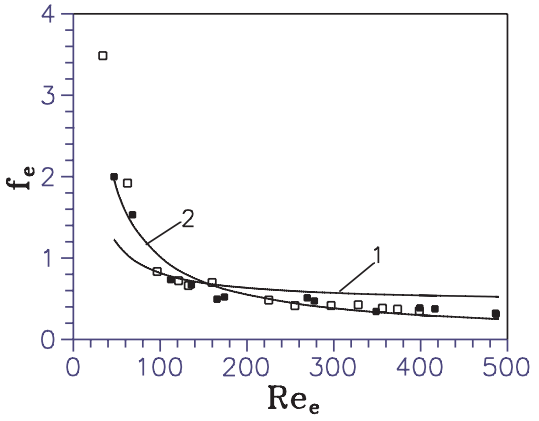

Fig. 14. MPHE friction factor: ■ – hot side; □ – cold side; 1 – Eq. (17); 2 – Eq. (18).

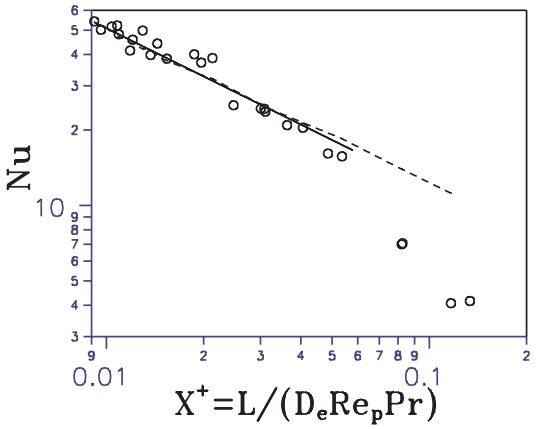

Fig. 15. Average Nusselt number for the porous-media heat-exchanger: --- Eq. (19); —— Eq. (20).

conventional packed beds have more than 10 layers of particles in a cross-section. Therefore, the friction factor calculated from the experimental data is expected to differ from that predicted by Eq. (17). The data for f_e can be correlated with Re_e as

$$f_e = 57.9/Re_e^{0.88} \quad (Re_e < 500). \tag{18}$$

The volumetric heat transfer coefficient in the MPHE is presented in Fig. 11 as a function of velocity for equal hot and cold side mass flow rates. Although the water flow rate range in the MPHE was relatively small, the heat transfer coefficient increased greatly with increasing flow velocity. The maximum water flow rate in the porous-media heat-exchanger was 0.067 kg/s, the corresponding average velocity was 1.06 m/s and the maximum volumetric heat transfer coefficient was 86.3 MW/(m^3 K), which is much higher than in the microchannel heat-exchanger, MHE1. The maximum volumetric heat transfer coefficient, K_V, in the MPHE is less than that in the MCHE manufactured by Bier, et al. [7] (324 MW/(m^3 K)). However, the overall heat transfer coefficient K_F of the MPHE based on the projected (flat) surface (60.4 kW/(M^2 K)) was higher than the overall heat transfer coefficient of the MCHE manufactured by Bier, et al. [7] based on the projected (flat) surface area (22.8 kW/(m^2 K)). This means that the heat transfer enhancement produced by the porous media with 0.272 mm particle diameter is greater than the heat transfer increase in the 0.1 mm wide and 0.078 mm deep microchannels used by Bier, et al. [7]. However, the MPHE in the present research is less compact than the MCHE manufactured by Bier, et al. [7].

The experimental average Nusselt number for the porous-media heat-exchanger decreases with increasing non-dimensional length X^+, Fig. 15. Fig. 15 also shows the Nusselt number predicted by the following empirical correlation for packed beds [33]:

$$Nu = (1 - d_p/D_e)\,Re_p^{0.61}\,Pr^{1/3} \quad (50 < Re < 2 \times 10^4). \tag{19}$$

For $X^+ < 0.05$, the experimental data and the correlation are very close, within ±10%.

However, for $X^+ > 0.05$, the experimental data is much less than the correlation, which may be due to uneven fluid distribution in the heat-exchanger channels for low mass flow rates, which would significantly decrease the heat transfer in the heat-exchanger. The experimental data can be correlated as

$$Nu = 1.97(Re_p\,Pr\,D_e/L)^{0.72} \quad (X^+ < 0.05). \tag{20}$$

The discrepancy between Eq. (20) and the experimental data is less than ±6%.

Fig. 16 presents the heat-exchanger effectiveness of the porous-media heat-exchanger for equal hot and cold side mass flow rates. The differences between the experimental data for the heat-exchanger effectiveness and the correlation, Eq. (16), are less than 5%. All of the

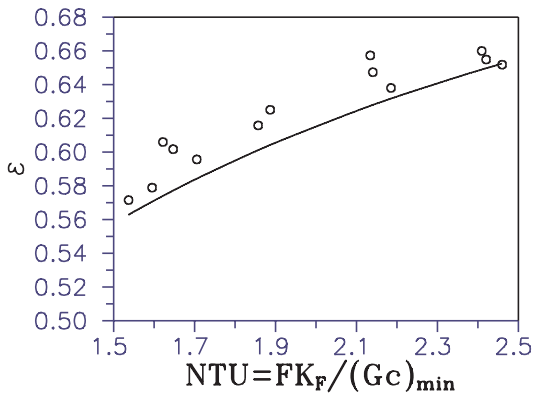

Fig. 16. Effectiveness of the cross-flow MPHE: ◯ – experimental results; —— Eq. (16).

experimental data for ε are a little higher than the correlation, which also may be caused by uneven hot and cold water mass flow rates. The heat-exchanger effectiveness in MPHE is higher than in MCHE.

4. Micro-heat-exchanger performance evaluation

Generally, heat-exchanger performance includes many aspects, e.g., heat transfer, flow resistance, mechanical and economical performance, etc. The present paper evaluates the performance of different types of micro-heat-exchangers based on heat transfer and flow resistance aspects.

The flow and heat transfer performance of MHE1 and MHE2 are compared with another micro-channel heat-exchanger, MHE3, and a conventional plate heat-exchanger, HE4, in Figs. 8 and 11 with water as the working fluid. The design parameters for MHE3 and HE4 can be found in [8,10,26].

The volumetric heat transfer coefficients, K_V, for these three micro-heat-exchangers are much better than for conventional plate heat-exchangers, Fig. 11. The increase of the volumetric heat transfer coefficient with velocity is similar for MHE1 (deep micro-channels) and MHE3 (shallow micro-channels), but K_V for MHE1 is less than K_V for MHE3. The volumetric heat transfer coefficient of MPHE is much higher than either MCHE. The volumetric heat transfer coefficient of the porous-media micro-heat-exchanger increases much more quickly with velocity than that of the micro-channel heat-exchangers, because of the thermal dispersion in porous media, which intensifies as the flow velocity increases [21]. Therefore, from the heat transfer point of view the porous-media micro-heat-exchanger has an obvious advantage.

However, as shown in Fig. 8, for the same flow rate the pressure drop in the MPHE (MHE2) is the largest, with successively lower pressure drops in MHE3, HE4, and MHE1. Comparison of MHE1 with MHE3 shows that the MCHE with deep micro-channels has a smaller pressure drop with a relatively large volumetric heat transfer coefficient. The maximum volumetric heat transfer coefficient was 38.5 MW/(m^3 K) for MHE1 with a pressure drop of 0.9 bar, while the maximum volumetric heat transfer coefficient was 44.5 MW/(m^3 K) for MHE3 with a pressure drop of 3.4 bar.

The ratio of the volumetric heat transfer coefficient, K_V, to the pump power, N, for the four heat-exchangers, Fig. 17, decreased from MHE1 to MHE3 to MHE2 to HE4, indicating that for this criterion, the MCHE with deep channels has better overall performance. The ratio of the volumetric heat transfer coefficient, K_V, to the pressure drop, Δp, is presented in Fig. 18. For the same flow rate, the values of $K_V/\Delta p$ for the micro-channel heat-exchanger with deep channels are higher than the micro-channel heat-exchanger with shallow channels and the porous media heat-exchanger. Therefore, the MCHE with deep channels has better overall thermal–hydraulic performance.

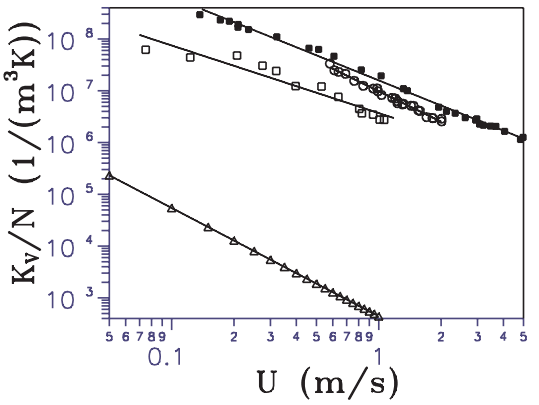

Fig. 17. Ratio of volumetric heat transfer coefficient to pumping power: ■ – MHE1; □ – MHE2; ◯ – MHE3; △ – HE4.

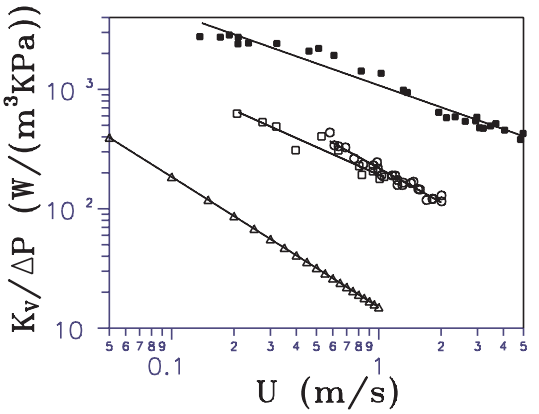

Fig. 18. Ratio of volumetric heat transfer coefficient to pressure drop: ■ – MHE1; □ – MHE2; ◯ – MHE3; △ – HE4.

Therefore, from the heat transfer point of view the micro-porous heat-exchanger is better than the micro-channel heat-exchangers, and the MCHE with shallow micro-channels is better than the MCHE with deep micro-channels. However, from the pressure drop point of view the MCHE with deep micro-channels is the best. The MCHE with deep channels has the best overall performance considering both the heat transfer and flow resistance.

5. Conclusion

Fluid flow and forced convection heat transfer in MCHE and MPHE was investigated theoretically and experimentally. The conclusions can be summarized as:

1. For the same flow rate, the pressure drop in the MCHE with deep channels is much lower than in the MCHE with shallow channels, but the difference between their heat transfer rates is not large. The maximum volumetric heat transfer coefficient in the MCHE with deep channels was 38.5 MW/(m^3 K) for water flow rate of 0.34 kg/s and a pressure drop of 0.9 bar.
2. The transition from laminar to turbulent flow in the micro-channel heat-exchanger occurs much earlier, at $Re \approx 600$, compared to usual fluid flow in large, smooth channels.
3. The MPHE has better heat transfer performance than the MCHE. The maximum water flow rate in the porous-media heat-exchanger was 0.067 kg/s, the corresponding maximum volumetric heat transfer coefficient was 86.3 MW/(m^3 K), and the pressure drop was 4.66 bar.
4. From the heat transfer point of view the MPHE is better than the MCHEs while the MCHE with shallow channels is better than the MCHE with deep channels. However, the MCHE with deep channels has the best overall thermal–hydraulic performance.

Acknowledgements

The project was financially supported by the National Natural Science Foundation of China (No. 59506004) and the Natural Science Fundamental Research Foundation of Tsinghua University, Beijing, China.

References

[1] D.B. Tuckerman, R.F.W. Pease, High performance heat sinking for VLSI, IEEE Electron. Device Lett. EDL2 (1982) 126–129.
[2] D.B. Tuckerman, Heat transfer micro-structures for integrated circuits, Ph.D. Thesis, Lawrence Livermore National Laboratory, UCRL-53515, 1984.
[3] M. Mahalingam, J. Andrews, High performance air cooling for micro-electronics, Cooling Technol. Electron. Equipment (1987) 121–136.
[4] P.Y. Wu, W.A. Little, Measurement of friction factors for the flow of gases in very fine channels used for micro-miniature Joule–Thomson refrigerators, Cryogenics 23 (5) (1983) 273–277.
[5] G.W. Swift, A. Migliori, T.C. Wheatley, Micro-channel flow fluid heat-exchanger and method for its fabrication, US Patent 4 (1985) 516–632.
[6] W. Cross, C. Ramshaw, Process intensification: laminar flow heat transfer, Chem. Eng. Res. Des.: Trans. Inst. Chem. Eng. 64 (1986) 258–294.
[7] W. Bier, W. Keller, G. Linder, D. Seidel, K. Schubert, Manufacturing and testing of compact micro heat exchangers with high volumetric heat transfer coefficients, Micro Structures, Sensors and Actuators, ASME DSC 19 (1990) 189–197.
[8] S.D. Kang, Micro cross-flow heat exchanger, Ph.D. Thesis, Louisiana Tech University, Ruston, LA, 1992.
[9] S. Wild, L.R. Oellrich, et al., Comparison of experimental and computed performance of micro heat exchangers in the ranges of LHE and LN2 temperatures, in: Heat Transfer 1994, Brighton UK, 1994, pp. 441–445.
[10] F.D. Friedrich, C.R. Kang, Micro heat exchangers fabricated by diamond machining, Precision Eng. 16 (1) (1994) 56–59.
[11] R.W. Keyes, Heat transfer in forced convection through fins, IEEE Trans. Electron. Devices Ed-31 (1984) 1218–1221.
[12] V.K. Samalam, Convective heat transfer in microchannels, J. Electron. Mater. 18 (5) (1989) 611–617.
[13] T.M. Harms, M.J. Kazmierczak, F.M. Gerner, Developing convective heat transfer in deep rectangular microchannels, Int. J. Heat Fluid Flow 20 (1) (1999) 149–157.
[14] S.V. Belov, V.A. Devisilov, V.N. Zhdanov, Hydraulic resistance of woven metal screens. Khimicheskoe I Neftyanoe Mashinostroenie 8 (1989) 26–28 (in Russian).
[15] P. Hsu, C.T. Cheng, Thermal dispersion in a porous medium, Int. J. Heat Mass Transfer 33 (8) (1990) 1587–1597.
[16] K. Vafai, M. Sozen, Analysis of energy and momentum transport for fluid flow through a porous bed, J. Heat Transfer 112 (1990) 690–699.
[17] M. Kaviany, Principles of Heat Transfer in Porous Media, Springer, New York, 1991.
[18] U.A. Jeigarnik, F.P. Ivanov, N.P. Ikranikov, Experimental data on heat transfer and hydraulic resistance in unregulated porous structures, Teploenergetika (2) (1991) 33–38 (in Russian).
[19] D.A. Nield, A. Bejian, Convection in Porous Media, Springer, New York, 1999.
[20] P.X. Jiang, Z.P. Ren, B.X. Wang, Numerical simulation of forced convection heat transfer in porous plate channels using thermal equilibrium and non-thermal equilibrium models, Numer. Heat Transfer Part A 35 (1999) 99–113.
[21] P.X. Jiang, Z. Wang, Z.P. Ren, Experimental research of fluid flow and convection heat transfer in plate channels filled with glass or metallic particles, Exp. Thermal Fluid Sci. 20 (1) (1999) 45–54.
[22] P.G. Zhu, Principle and Calculation of Heat Exchanger, Tsinghua University Press, Beijing, 1991 (in Chinese).
[23] M.K. Alkam, M.A. Al-Nimr, Improving the performance of double-pipe heat exchangers by using porous substrates, Int. J. Heat Mass Transfer 42 (1999) 3609–3618.
[24] P.X. Jiang, Z.P. Ren, B.X. Wang, Micro-scale heat and mass transfer and micro heat exchanger, Prog. Micro/Nano Technol. (1996) 115–119 (in Chinese).
[25] P.X. Jiang, B.X. Wang, Z.P. Ren, Micro heat exchanger and relevant problems, J. Eng. Thermophys. 17 (3) (1996) 328–332 (in Chinese).
[26] M.H. Fan, Micro heat exchangers, Master's Thesis, Tsinghua University, Beijing, 1998 (in Chinese).
[27] W.M. Kays, A.L. London, Compact Heat Exchangers, McGraw-Hill, New York, 1993.
[28] Gh.M. Mala, D.Q. Li, Flow characteristics of water in microtubes, Int. J. Heat Fluid Flow 20 (1) (1999) 142–148.

[29] B.S. Petukhov, L.G. Genin, S.A. Kovalev, Heat Transfer in Nuclear Power Equipment, Energoatomizdat Press, Moscow, 1986 (in Russian).
[30] P. Wibulswas, Laminar flow heat transfer in non-circular ducts, Ph.D. Thesis, London University, London, 1966.
[31] F.P. Incropera, D.P. DeWitt, Fundamentals of Heat Transfer, third ed., Wiley, Singapore, 1990.
[32] M.E. Aerov, O.M. Tojec, Hydraulic and Thermal Basis on the Performance of Apparatus with Stationary and Boiling Granular Layer, Himia Press, Leningrad, 1968 (in Russian).
[33] E. Achenbach, Heat and flow characteristics of packed beds, Exp. Thermal Fluid Sci. 10 (1) (1995) 17–27.